Available online at www.sciencedirect.com

jmr&t Journal of Materials Research and Technology

www.jmrt.com.br

Original Article

Phosphorization of exfoliated graphite for developing flame retardant ethylene vinyl acetate composites

Ghane Moradkhani[a], Mohammad Fasihi[a,*], Thibault Parpaite[b], Loic Brison[c], Fouad Laoutid[c], Henri Vahabi[d], Mohammad Reza Saeb[e]

[a] School of Chemical Engineering, Iran University of Science and Technology, Tehran 16846-13114, Iran
[b] Precision Macromolecular Chemistry Group, Institut Charles Sadron, CNRS-UPR 22, 23 rue du Loess, 67034, Strasbourg, Cedex 2, France
[c] Polymeric and Composite Materials Unit, Materia Nova Research Center, Nicolas Copernic 3, 7000, Mons, Belgium
[d] Université de Lorraine, CentraleSupélec, LMOPS, F-57000 Metz, France
[e] Department of Resin and Additives, Institute for Color Science and Technology, P.O. Box, 16765-654, Tehran, Iran

ARTICLE INFO

Article history:
Received 4 March 2020
Accepted 26 April 2020

Keywords:
Poly (ethylene-co-vinyl acetate)
Exfoliated graphite nanoplatelet
Functionalization
Flame retardancy
Mechanical properties

ABSTRACT

Ammonium polyphosphate (APP) was grafted onto the surface of exfoliated graphite nanoplatelet (GNP) to obtain a novel flame retardant, GNP-g-APP, and thereafter was incorporated into the ethylene vinyl acetate (EVA) to improve its flame retardancy. The chemical structures of the precursors and the target product were characterized by Fourier transform infrared spectroscopy (FTIR), scanning electron microscopy (SEM), thermogravimetric analysis (TGA), and energy dispersive X-ray spectroscopy (EDS) techniques. FTIR spectra appeared at 1056 and 1103 cm^{-1} were attributed to P—O—C asymmetric stretching bond, that conformed formation of GNP-g-APP. Thermal stability behaviour and flame retardancy performance of the samples were evaluated by TGA, UL-94, micro-calorimetry, and cone calorimetry. TGA measurements revealed the superiority of GNP-g-APP over GNP. The micro-calorimetry analyses indicated a sharp fall in both the total heat release (THR) and the peak of heat release rate (pHRR) of EVA containing 30 wt.% GNP-g-APP, evidenced by a thick char layer formed as barrier. Cone calorimetry confirmed flame-retardant effect of GNP-g-APP featured by a reduction in pHRR (−63 %) and THR (−31.6 %) due to the formation of a cohesive char layer. Although GNP addition sharply decreased the elongation at break of 70/30 (w/w) composites from 500% for neat EVA to 71%, a very promising value of 364% for EVA/GNP-g-APP sample preserved superior flexibility.

1. Introduction

Copolymer of ethylene and vinyl acetate, poly (ethylene-co-vinyl acetate) (EVA) was broadly applied in biomedical [1], construction [2], packaging [3], and electrical industries,

* Corresponding author.
E-mail: mfasihi@iust.ac.ir (M. Fasihi).
https://doi.org/10.1016/j.jmrt.2020.04.085

mainly as hot-melt adhesive [4] and electrical cable [5], but it appeared flammable [5–9]. Halogenated flame retardants have been selected as common additives for high flammable polymers [10], but their usage was banned/limited due to the emission of toxic and corrosive gasses [11]. To tackle this problem, a wide variety of additives/fillers such as alumina trihydrate (ATH) and magnesium hydroxide (MDH) have been examined. Nevertheless, such minerals could have been used at high loadings (~30–60%) that would have detrimental effects on the mechanical properties of composites [12–14]. Thus, using reactive materials like expandable graphite (EG) and ammonium polyphosphate (APP) at low loading received more attention [15,16].

In recent years, carbon-based materials have been widely considered for their adequate flame retardant properties [17,18]. For instance, by studying the thermal and flame retardant properties of three kinds of graphite structures (natural graphite, EG, and graphene oxide), Wu et al. uncovered promising effect of EG on the EVA through the formation of carbon layers within which sulphuric acid (H_2SO_4) appeared as intercalated structure [19]. When EG was heated, it could expand, approximately by 100 times, along the C axis of its crystal structure to create a protective physical layer on the polymer matrix [20]. The resulting physical protective layer assisted in reduction of heat and gas transfer in the course of combustion [21–23]. However, unaccompanied use of EG had two disadvantages: first, the incompact structure of the char layers could easily be blown off by the turbulence of flame impingement [24]; second, the poor compatibility between EG and polymer matrix deteriorated the mechanical properties of composites [25]. Therefore, many researches attempted to modify graphite by increasing its adsorptive capacity, e.g. with $MgCl_2{\cdot}6H_2O$ [26], functionalizing graphene nanoplatelet to enhance thermal performance of wind turbines [27], functionalizing EG for adsorption of methyl orange [28], and anchoring carboxyl groups on the graphite to make it hydrophilic and enhance electrolyte wettability properties [29]. Most of the works done to improve the flame retardant performance of graphite were based on the physical combination of EG with other flame retardants, e.g. aluminium hydroxide [30], ammonium polyphosphate [31], red phosphorus [21] and phenylphosphinic [32] to obtain synergistic effects. One of the few works on chemical modification of exfoliated graphite nano-platelets was the one due to Wang et al. who introduced a covalently grafted 910-dihydro-9-oxa-10-phosphaphenanthrene-10-oxide (DOPO) onto graphite [33]. They applied their product in polyethylene and improved the total heat release (THR) form125 to 85.6 MJ/m^2, while limiting oxygen index (LOI) from 17.5 to 30.6% at 20 wt.% of EG-g-DOPO.

Phosphorus-based materials are known as effective flame retardants by representing different degrees of oxidation including phosphates, phosphonates, phosphinates [34,35]. These materials, when exposed to fire, reduce the amount of fuel by formation of char during combustion, capturing free radicals, and preventing the release of gases to vapour phase. As a result, they reduce combustibility, and insulate polymers against heat. APP is a phosphorus-containing flame retardant that contains both acid source and blowing agent, which has been used to make EVA flame retardant [36]. Up to now, a variety of phosphorus derivatives highly efficient halogen-free flame retardants (FRs) have been functionalized with graphene to enhance the flame-resistant efficiency of graphene [37–40]. Ran et al. [41] reported that graphene functionalized with (DOPO) and branched polyethylenimine (BPEI) could improve the specific extinction area (ASEA) and the total smoke release (TSR) of polylactic acid (PLA). Shao et al. [42] reported that modification of APP via ion exchange reaction with ethylenediamine increases charring efficiency. Modification of APP for polyamide (PA) has led to a-80-percent fall in the value of pHRR of PP containing 25 wt.% PA-APP by comparison with the neat PP. However, inadequate mechanical properties of flame retardant EVA highly filled with exclusive additives from one side and the need for developing a flame retardant acting at low loading through a facile synthesis route and based on available commercial FRs from the other side have remained an unanswered question.

In this work, a phosphorus-containing flame retardant, namely GNP-g-APP, was prepared via functionalization of exfoliated graphite nanoplatelet (GNP). Fourier transform infrared (FTIR), scanning electron microscopy (SEM), thermogravimetric analysis (TGA) and energy dispersive X-ray spectroscopy (EDS) were employed to probe into the structure of GNP-g-APP. The resulting GNP-g-APP was applied as a flame retardant to the EVA polymer matrix. The thermal degradation and flammability of EVA/GNP and EVA/GNP-g-APP composites were investigated by TGA and pyrolysis combustion flow calorimetry (PCFC). Mass loss cone calorimetry was also performed to provide an image of flame retardancy performance of the developed composite in terms of well-known parameters [43]. Mechanical properties of EVA composites containing GNP and GNP-g-APP were also compared with that of EVA using tensile test to give useful insights into the compatibility of the used flame retardant additives with EVA.

2. Experimental

2.1. Materials

EVA was commercial grade of EVA 1316 with vinyl acetate content of 18 wt.% having melt flow rate (MFR) of 0.8 g/10 min purchased from Hanwa Chemical, South Korea. EG nanosheets having expansion ratio of 200 $cm^3\,g^{-1}$ and an average particle size above 300 nm) was obtained from Ito Kokuen Co, Japan. Pristine form of commercial APP supplied by Kimia Pooyesh, Iran was used as phosphorus flame retardant. NaOH and ethanol were purchased from Merck Co, Germany, and used as received.

2.2. Preparation of GNP-g-APP

EG powder was annealed in a furnace for 30 s at 900 °C. APP was dried at 105 °C for 12 h in an oven. The prepared exfoliated graphite nanoplatelet (GNP) and APP powders were used as the initial materials and mixed in 5:1 wt ratio using ball-milling for 8 h. After that, the mixture together with 20 g of NaOH were added into a three-neck flask containing ethanol (99.9%) under stirring and nitrogen atmosphere. Afterwards, the mixture was heated at 90 °C, the reaction temperature preserved for about 10 h. The resulting solid was rinsed, over

Table 1 – EVA and its graphitic composites.

Samples	EVA	GNP	GNP-g-APP
EVA	100	–	–
EVA/GNP30	70	30	–
EVA/GNP-G-APP30	70	–	30

and over again was sieved under vacuum, and washed three times with ethanol solvent. Then, it was washed with deionized water to have a pH around 6. Finally, the resulting powder (GNP-g-APP) was dried at 105 °C in a vacuum oven overnight.

2.3. *Sample preparation*

EVA pellets were melt-mixed with the GNP and GNP-g-APP powders separately at fixed loading of 30 wt. % in an Xplore conical twin-screw micro-compounder (MC 15 HT, Netherlands) at 120 °C and a rotor speed of 60 rpm for 10 min (Table 1). All blends were grinded, then hot pressed and molded using an Agila machine under 80 bars at 120 °C for 20 min to obtain the specimens in the form of square sheets ($100 \times 100 \times 4\,mm^3$) for cone calorimeter analysis. For preparing specimens of UL-94 and mechanical properties tests, since the melt mixing was completed, the melt polymer composites underwent calendering to prepare thin films by using a casting machine (Xplore thickness: 0.5 mm, width: 15 mm).

2.4. *Characterization methods*

FTIR measurements were conducted on a Jasco FTIR 615, Jasco Inc., (USA). The GNP and GNP-g-APP samples in the form of powder (grinded product of compounds obtained from micro-compounder) were pressed into KBr pellets by compression to collect FTIR spectra with resolution of $4\,cm^{-1}$ varying wavelength between 4000 and $400\,cm^{-1}$.

Thermal decomposition behaviour of samples having weight of 10 ± 2 mg was studied through thermogravimetric analysis (TGA) on a Setaram Labsys Evo thermogravimetric analyser (France) under nitrogen atmosphere keeping the heating rate fixed at $10\,°C\,min^{-1}$.

A scanning electron microscope, FEI Quanta 200 SEM (USA) was used to study the microstructure of samples. The apparatus was equipped with a high-vacuum chamber working at a voltage of 10 kV, keeping spot size fixed at 4 and probe distance at 8–10 mm. SEM micrographs were provided from carbon-sputtered cryogenically fractured EVA and EVA composites.

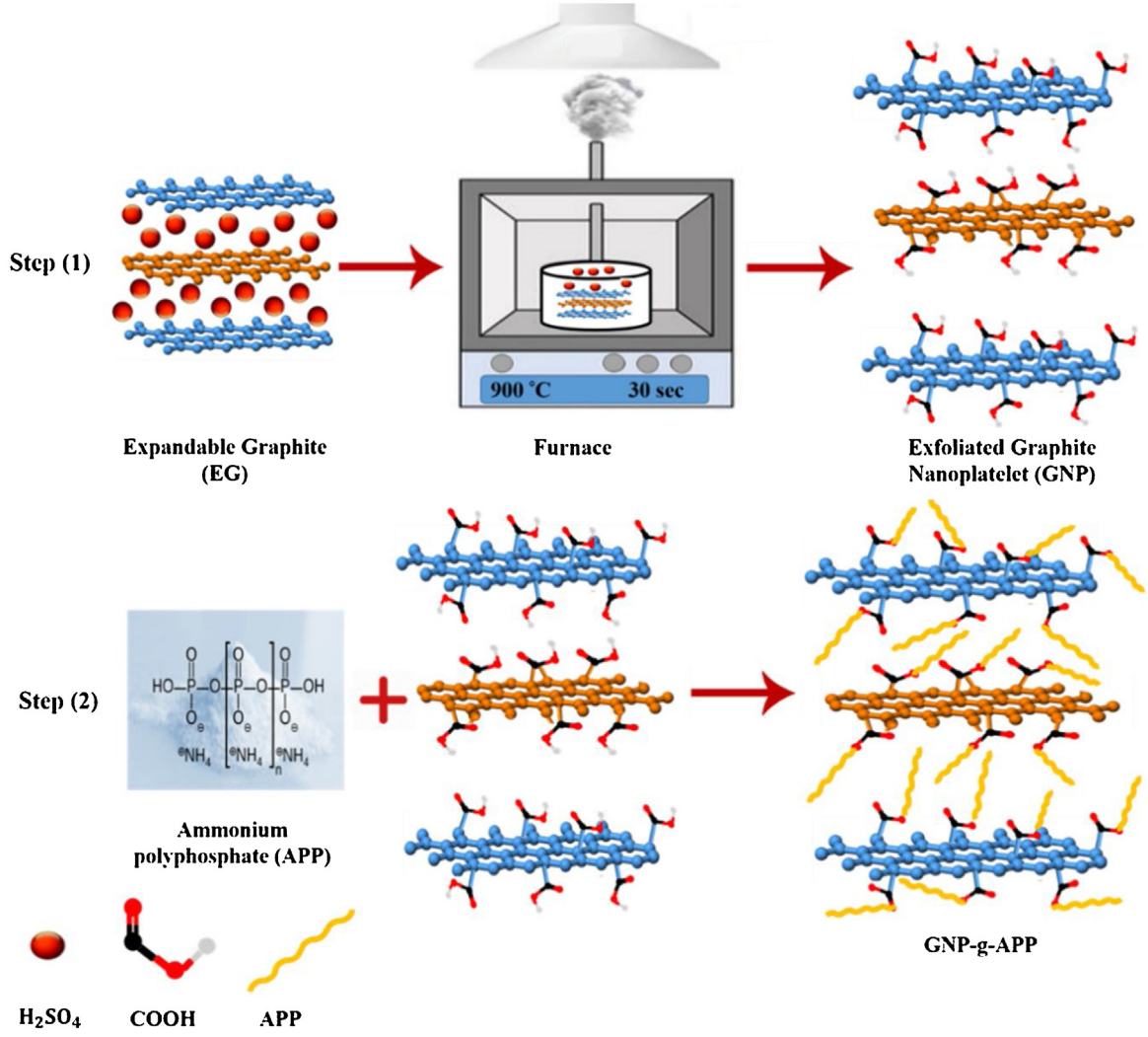

Scheme 1 – Possible reaction between GNP and APP.

A set of experiments were done to study fire retardancy behavior of samples. First, UL-94 was carried out in accordance with ASTM D3801 as a rough estimation to study burning of specimens of $120 \times 15 \times 0.5\,mm^3$ dimension in a vertical manner. The flammability of samples was studied by a micro-calorimetry analysis on a PCFC apparatus. To do so, about 2 mg of each sample underwent pyrolysis at 750 °C in nitrogen atmosphere by heating samples under the rate of $1\,°C\,s^{-1}$. The apparatus worked on the basis of transfer of gases released during the pyrolysis into a combustion chamber containing 20% oxygen to be completely oxidized at 900 °C. Each test was repeated three times and the mean values of PCFC characteristics, including the total heat release (THR), the peak of heat release rate (pHRR), and the temperature at which pHRR takes place were recorded. The analysis made by PCFC provides the researcher with a basic knowledge about flammability of samples, but the outcome cannot be generalized to a semi-real condition. Therefore, the fire behaviours of EVA and its nanocomposites were studied on a mass loss cone calorimeter (MLC) apparatus in accordance with the ISO 13927 procedure. As per instruction, small sheets of $100 \times 100 \times 4\,mm^3$ dimension were prepared by compression moulding and placed in the combustion chamber giving them exposure to irradiation of a mild external heat flux of $35\,kW/m^2$. The main characteristics of the tests including THR, heat release rate (HRR) as a function of burning time, pHRR, and the time to ignition (TTI) were directly collected for the sake of comparison of fire retardancy of samples.

Mechanical properties of neat EVA and its nanocomposites were studied under tension. Tensile measurements were carried out on a SANTAM Universal Testing Machine in accordance with ASTM D638 procedure. Samples of $45 \times 15 \times 0.5\,mm^3$ obtained by calendering of molten composites extruded by micro-compounder underwent tension at a crosshead speed of $10\,mm/min^{-1}$.

3. Results and discussion

3.1. *Characterisation of GNP-g-APP*

3.1.1. *FTIR analysis*

The FTIR spectra of the GNP and GNP-*g*-APP nanosheets are compared in Fig. 1. For GNP, the peaks at 3439, 2925 cm^{-1} can be ascribed to the O—H stretching, while the peaks at 1729, 1632, 1255 and 1077 cm^{-1} respectively belong to the stretching vibration of carbonyl, C=C, C—OH and C=O [33,44,45]. FTIR spectrum of GNP-g-APP shows a peak at 1296 cm^{-1} corresponding to the stretching vibration of P=O. Once modification by APP performed, two new peaks appeared in GNP-g-APP at 1056 and 1103 cm^{-1} attributed to P—O—C asymmetric stretching bond (see Scheme 1). As shown in Fig. 1, the intensity of the OH bond (at 2925 and 3439 cm^{-1}) in the FTIR spectrum of GNP-*g*-APP was decreased because of the formation of P—O—C bond [42,46].

3.1.2. *Morphological observations*

The microstructure of GNP and GNP-*g*-APP were imaged (Fig. 2). Fig. 2a and b show overlapped layers of EG. Due to the effect of heat, the graphite layers after exposure to heat were

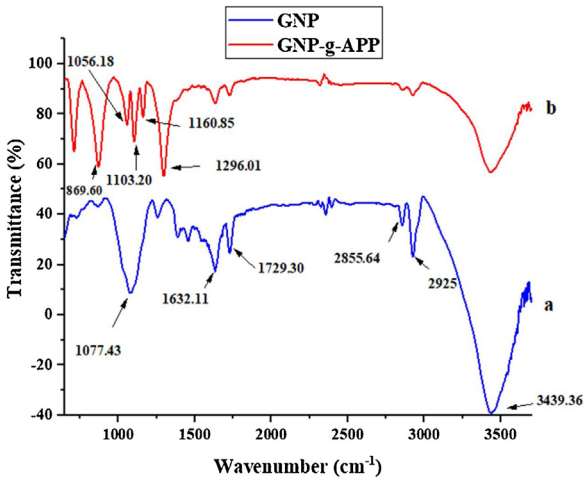

Fig. 1 – FTIR adsorption spectra of (a) GNP, and (b) GNP-*g*-APP.

significantly enlarged up to almost 100 times higher than that of the layers of untreated GNP, which made evidence for the increased volume of GNP in Fig. 2(c,d). This phenomenon was due to the hexagonal carbon structure of GNP and intercalated chemical compound (H_2SO_4) [18]. When the EG was placed inside the furnace at 900 °C, H_2SO_4 was oxidized, and decomposed into gases (CO_2, SO_2, and H_2O), which were responsible for the expansion. This is shown in the following reaction scheme [24]:

$$C + 2H_2SO_4 \rightarrow CO_2 + 2H_2O + 2SO_2 \quad (1)$$

The high pressure caused by the breakdown of intercalated zones made separated the graphite layers. Apparently, such an external pressure was much stronger than the binding forces between the graphite layers.

It is also interesting to note that after synthesis of GNP-*g*-APP, the structure was destroyed as shown in Fig. 3 and wrinkles were created on the surface and edges of the platelets.

Fig. 4 provides an overall view at a magnification of 20 μm on the white zones which are indicative of the presence of phosphate derivatives on the graphite surface. The energy dispersive X-ray spectroscopy (EDS) was done as a complement to SEM analyses (Fig. 5). It is clear that carbon, oxygen, and phosphorus elements are the main proportion of surface and are well dispersed, which is consistent with the results of the table inside the EDS of Fig. 5. Notably, the amount of phosphorus in the GNP-g-APP mentioned in the table reached 6.5 wt.%.

3.1.3. *Elemental analysis of GNP-g-APP*

The elemental mapping of carbon (C), oxygen (O), sodium (Na), phosphorus (P), and nitrogen (N) of GNP-g-APP are shown in Fig. 6. It is apparent that the P element was uniformly distributed at the surface of GNP-g-APP. A small amount of nitrogen was also dispersed, which was the result of the presence of non-reacted ammonium.

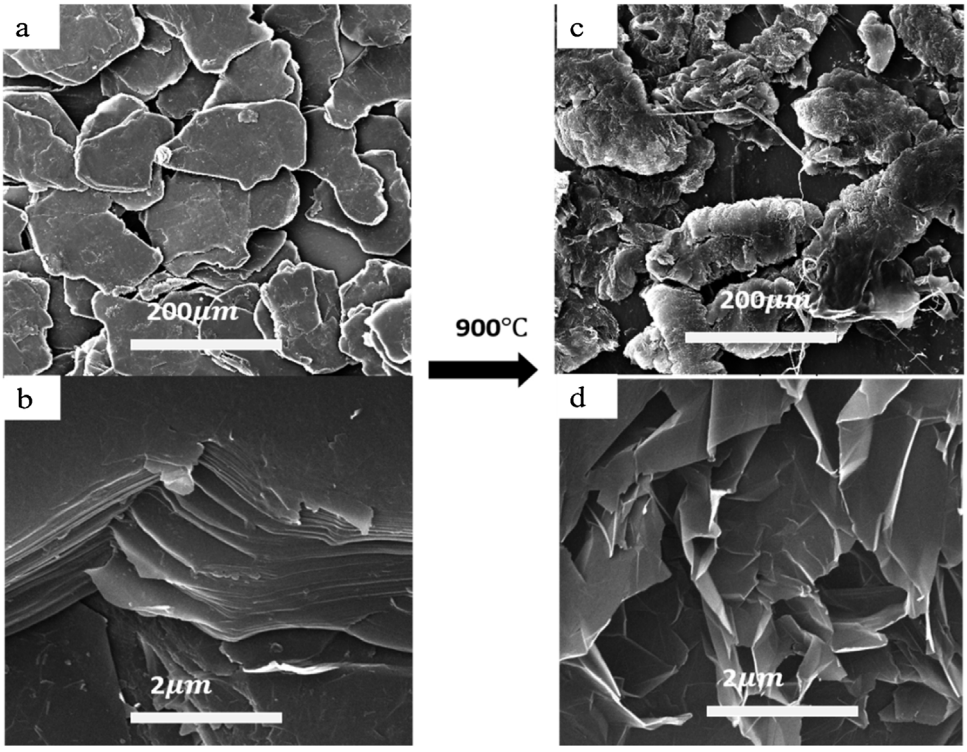

Fig. 2 – SEM images of EG (a, b) and GNP after being placed in the furnace (c, d).

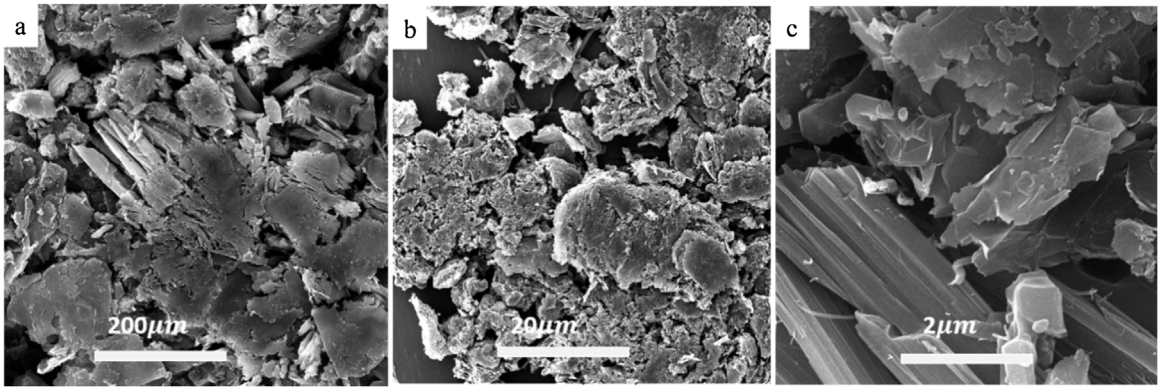

Fig. 3 – SEM images of GNP-*g*-APP (a, b and c).

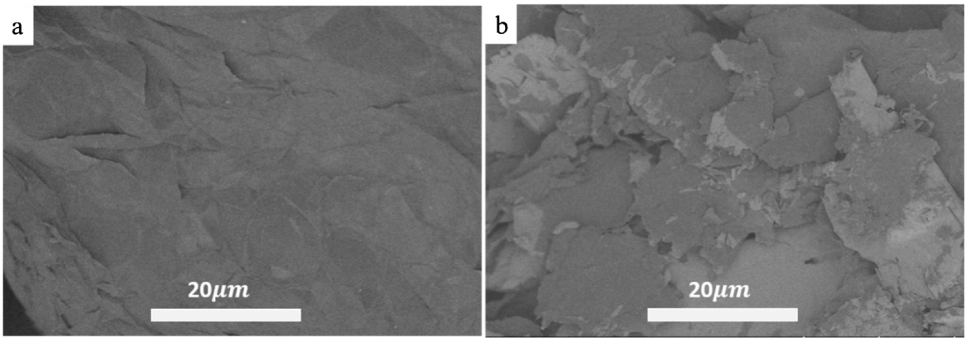

Fig. 4 – SEM back scatter electron images of GNP (a) and GNP-*g*-APP (b).

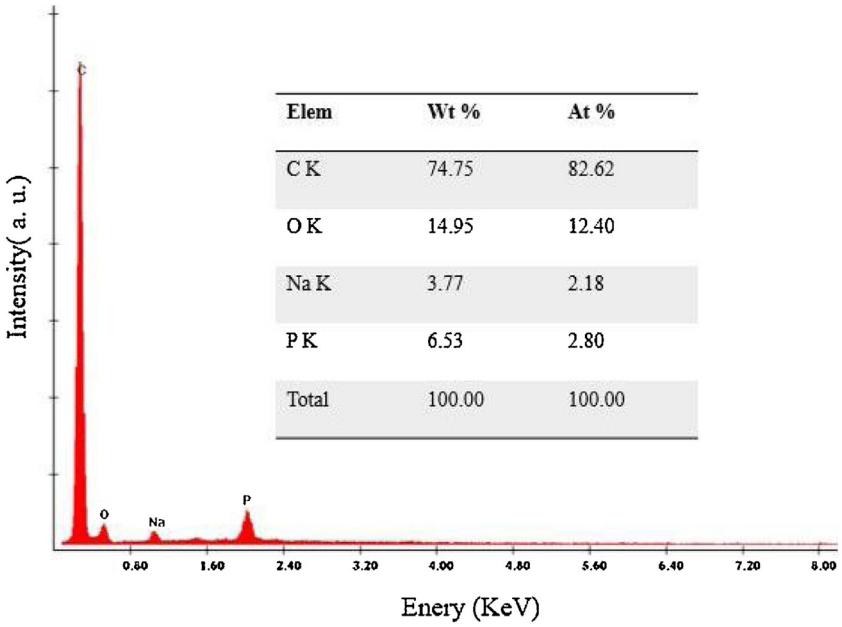

Elem	Wt %	At %
C K	74.75	82.62
O K	14.95	12.40
Na K	3.77	2.18
P K	6.53	2.80
Total	100.00	100.00

Fig. 5 – Energy dispersive X-ray spectroscopy (EDS) analysis data of GNP-*g*-APP.

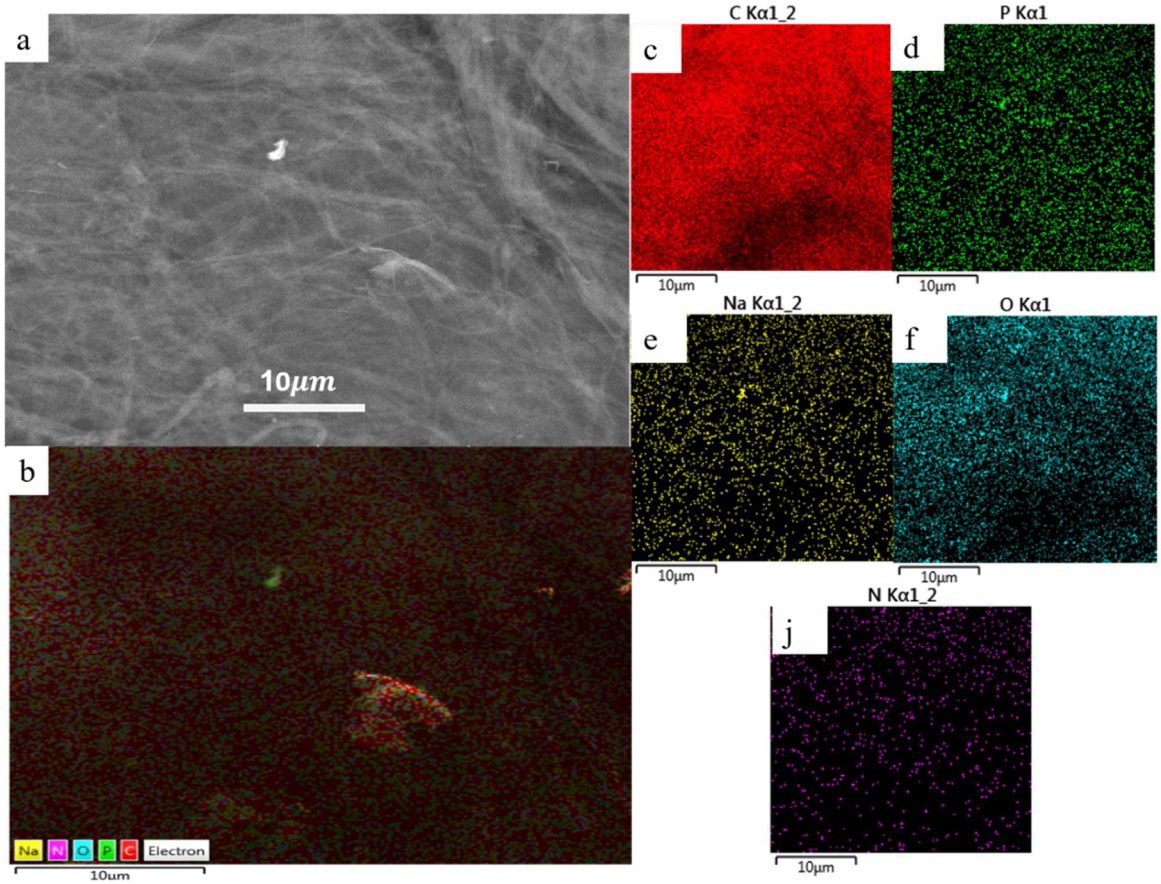

Fig. 6 – SEM image of GNP-g-APP (a), elemental mapping of GNP- g-APP (b), carbon (c), phosphorus (d), oxygen (e), sodium (f), and nitrogen (j).

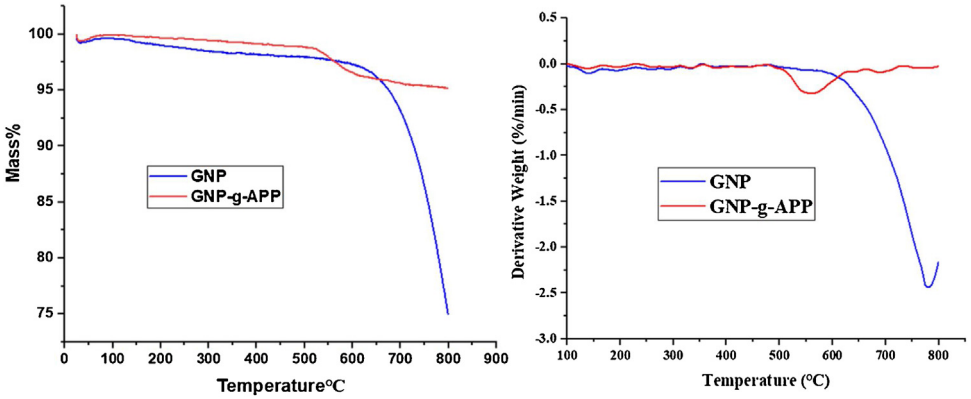

Fig. 7 – TGA and DTG curves of GNP and GNP-g-APP at heating rate of 10 °C min^{-1} under nitrogen atmosphere.

Table 2 – Analysis and data on TGA and DTG analyses at heating rate of 10 °C min^{-1} under nitrogen.

Sample code	$T_{5\%}$ (°C)	T_{max} (°C)	Residue (wt.%) at 800 °C
GNP	675	791	75
GNP-g-APP	>800	550	95
EVA	335	347–475	0
EVA/GNP30	337	353–472	26
EVA/GNP-g-APP	329	356–474	31

3.1.4. *Analysis of thermal behaviour of GNP and GNP-g-APP*

The TGA and derivative of TGA (DTG) curves of GNP and GNP-*g*-APP taken from cryogenically fractured samples are shown in Fig. 7. Moreover, the temperatures at which the relative mass loss of 5% ($T_{5\%}$), and the maximum mass loss (T_{max}) took place are summarized in Table 2. The $T_{5\%}$ of GNP is 675 °C, whereas that of GNP-*g*-APP is above 800 °C. The weight loss of GNP-*g*-APP stems from the decomposition of APP that releases phosphoric, polyphosphoric, and metaphosphoric acids [47]. The peak observed at 550 °C monitored in the DTG curve of GNP-*g*-APP can be ascribed to degradation of polyphosphate network [47]. Beyond 700 °C, the platelets of the GNP-*g*-APP could form barricades to block the pathway of volatile gases, but in the meanwhile some intermediates were probably formed that could weaken thermal resistance of GNP-*g*-APP. The char residue of GNP-*g*-APP was ca. 95% at 750 °C, well above that of GNP (75%). The thermal decomposition of APP promotes GNP to form a compact char layer under high temperature. As a result, the GNP-*g*-APP revealed higher thermal stability at elevated temperatures with respect to the GNP.

3.2. *Characterization of EVA and EVA composites*

3.2.1. *Morphological images*

The SEM micrographs of EVA composite specimens are shown in Fig. 8. Fig. 8a and b refer to EVA/GNP30 sample; while 8c and d correspond to EVA/GNP-g-APP30 sample. The presence of EG layers is clearly visible in the structure of composites.

3.2.2. *TGA and DTG curves*

The TGA and DTG curves of the neat EVA and EVA composites are shown in Fig. 9. Table 2 summarizes the results of $T_{5\%}$, T_{max}, and the residue amount at 800 °C. Overall, both the neat EVA and EVA/GNP30 composite underwent a clear two-step weight loss featured by sharp peaks of degradation, while for EVA/GNP-g-APP30 composite an almost broad peak was appeared in the first step, demonstrating complexity of degradation (see DTG curve in Fig. 9). The first weight loss for all samples occurred in between 300 and 380 °C, which can be attributed to thermal deacetylation of EVA chains [48]. The $T_{5\%}$ of EVA/GNP30 was 353 °C, above 347 °C detected for the neat EVA. The resistance of EVA/GNP30 compared to the neat EVA has been signalled by a slighter decay-type behaviour in TGA curve of the assigned sample in the first degradation step compared to that of EVA (see TGA curve in Fig. 9). The thermal stability of EVA/GNP-g-APP30 was slightly improved by broadening of the peak of degradation of the assigned sample (signature of higher thermal resistance) compared to that of EVA/GNP30 (see DTG curve in Fig. 9). On the other hand, the second degradation step taking place above 400 °C revealed a significant difference between thermal stability of samples. Typically, this behaviour could be attributed to the vinyl bond degradation and the volatilization of the residue. Although EVA was completely degraded at elevated temperatures, EVA/GNP30 and more remarkably EVA/GNP-g-APP30 resisted against thermal degradation as a result of the presence of mineral and organic compounds. The chemical bond between APP and GNP previously detected in Fig. 1 was the reason why the EVA/GNP-g-APP30 composite appeared thermally more stable. In agreement with this observations, the residue at 800 °C was increased from 26 wt.% for EVA/GNP30 to

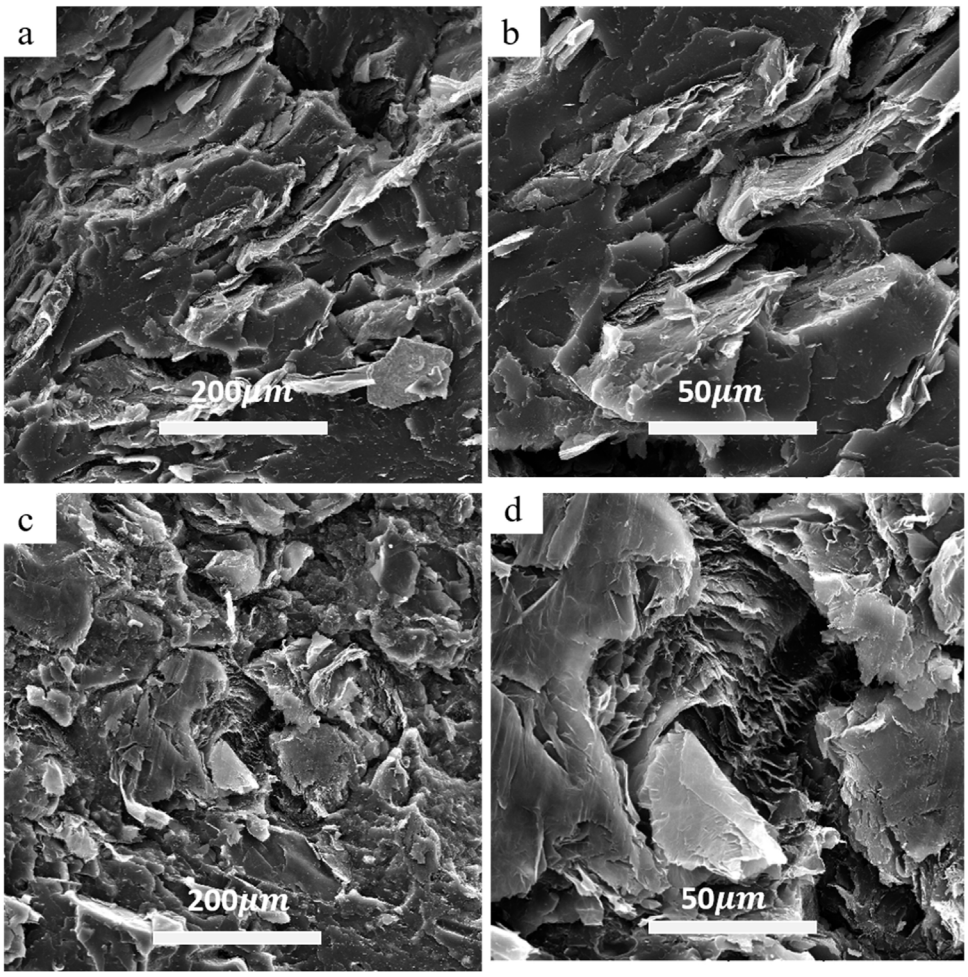

Fig. 8 – SEM images of EVA/GNP30 (a, b) and EVA/GNP-g-APP30 (c, d) composites.

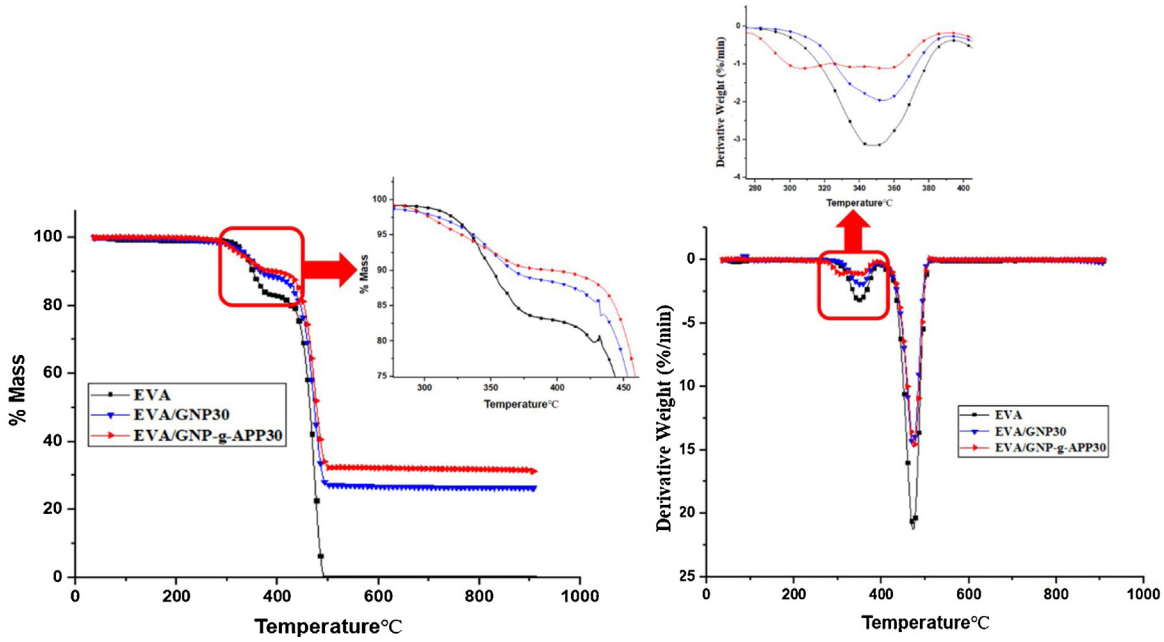

Fig. 9 – TGA and DTG curves of EVA, EVA/EG30, and EVA/GNP-*g*-APP30 at heating rate of 10 °C min^{-1} under nitrogen atmosphere.

Table 3 – Result of UL-94 of EVA samples.

Samples	UL-94	Dripping	Cotton ignition
EVA	NC[a]	Yes	Yes
EVA/GNP30	NC	Yes	Yes
EVA/GNP-g-APP30	V-0	Yes	No

[a] NC refers to not classified case in UL-94 test.

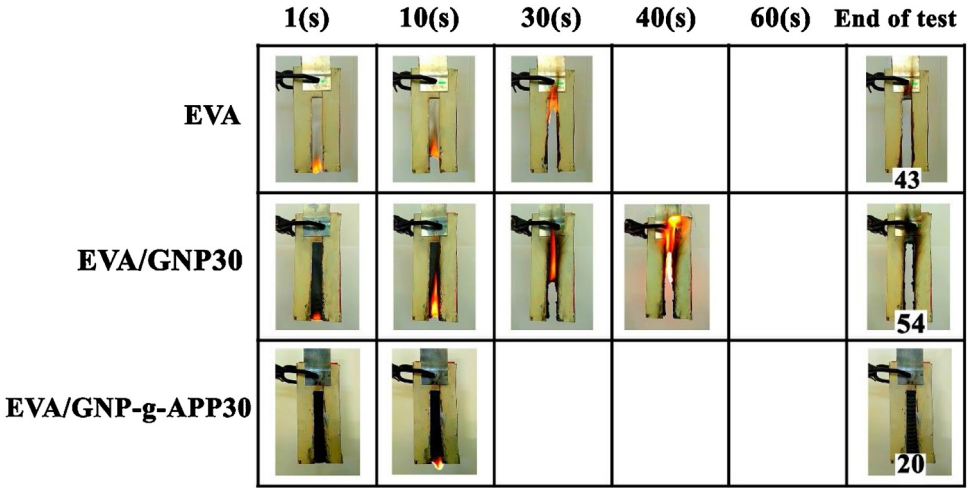

Fig. 10 – Digital photographs of EVA, EVA/GNP30, and EVA/GNP-g-APP30 during and after the vertical burning test.

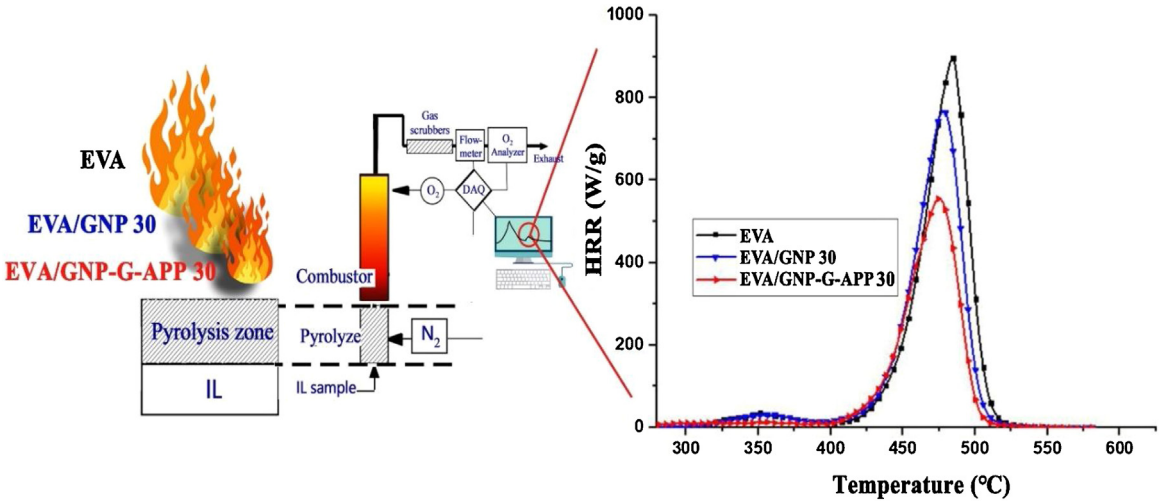

Fig. 11 – pHRR curves of EVA, EVA/GNP30, and EVA/GNP-g-APP30 at heating rate of 10 °C min^{-1} in nitrogen atmosphere.

31 wt.% for EVA/GNP-g-APP30 sample, implying that the GNP-g-APP promoted charring effect.

3.2.3. *UL-94*

The results of UL-94 test indicated that the neat EVA and EVA/GNP30 were highly flammable, for they were entirely burned from the bottom to the top of the holding clamp. Table 3 shows that all samples were dripped when exposed to flame. Moreover, the neat EVA and EVA/GNP30 have taken not classified (NC) label in UL-94 rating. By contrast, EVA/GNP-g-APP30 sample was not ignited even after 2 times by the exposure to the direct flame. For this sample, the cotton did not burn because of the incorporation of APP flame retardant. Therefore, this sample took V-0 rating label. To make sense of burning behaviour of samples, digital photographs provided from EVA, EVA/GNP30, and EVA/GNP-g-APP30 samples after the vertical burning test are displayed in Fig. 10.

3.2.4. *PCFC and PCFC-TGA superposition analyses*

The main characteristics of PCFC test were extracted from heat release-temperature scans for neat EVA and EVA composites (Fig. 11). The values of pHRR (W/g), maximum temperature (T_{pHRR}), THR (kJ/g), and heat release capacity, HRC (J/g K), are summarizes in Table 4. Both the neat EVA and EVA/GNP30

Table 4 – Result of PCFC analysis of EVA samples.

Name	$pHRR_1$ (W/g)	$pHRR_2$ (W/g)	T_{pHRR1} (°C)	T_{pHRR2} (°C)	THR (kJ/g)	HRC (J/(g K))	sum pHRR (W/g)	Reduction in pHRR with respect to EVA (%)
EVA	33	896	356	463	35	1040	930	–
EVA/GNP30	31	729	354	478	31	923	761	18
EVA/GNP-g-APP30	–	555	–	474	24	729	555	40

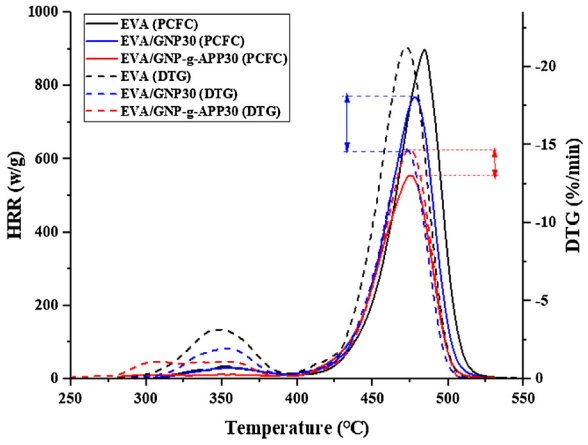

Fig. 12 – Superposition of HRR (solid lines), obtained from PCFC tests, and DTG (dashed lines) curves as a function of temperature for all samples.

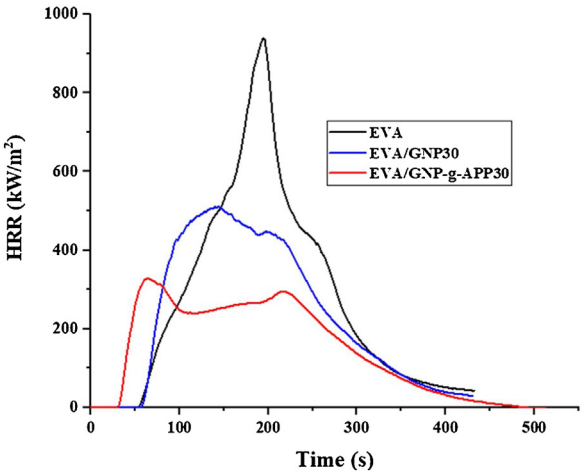

Fig. 13 – HRR curves of pristine EVA and composites (35 kW/m²).

samples exhibited two small peaks of HRR around 350 °C due to the loss of acetic acid and degradation of the ethylene repeating units of the backbone [49]. This is consistent with the results obtained by the TGA analysis (Fig. 9). In the case of EVA/GNP-g-APP30, the first peak of HRR was considerably decreased. All samples showed a second peak of HRR around 460 °C.

THR value of EVA was decreased from 35 to 31 kJ/g for EVA/GNP30 and 24 kJ/g for EVA/GNP-g-APP. The reduction in pHRR value of EVA/GNP30 and EVA/GNP-g-APP30 compared to neat EVA reached 18 and 40%, respectively. This suggest the efficiency of GNP-g-APP in reducing pHRR compared to GNP.

Fig. 12 compares the superposition of DTG (obtained from TGA tests, dashed line) and HRR (obtained from PCFC tests, solid line) curves for the neat EVA and EVA composites. The shapes of the curves obtained under nitrogen were similar. However, temperature dependency of HRR and DTG curves were different because of difference between heating rates applied in TGA and PCFC analyses.

Overall, a significant difference between degradation behaviour of samples can be seen in the first step of thermal decomposition. All peaks in DTG are higher than that of PCFC. This difference means that the quantity of degraded materials in DTG was not proportional to the amount of energy released by the gases. In the other words, the proportion of energy of gases released in the first step of thermal degradations was not significant compared to the whole amount of energy caused by released gases. For the second peak of HRR, the shape of PCFC and DTG curves and their peak loci and height were almost the same as those of neat EVA. However, some differences between curves should be noticed in view of thermal stability. For instance, the peak of HRR for EVA/GNP30 sample was positioned higher than that of DTG for this sample in the second step of decomposition, while an opposing trend was the case for EVA/GNP-g-APP30. Such contradictive thermal behaviours were possibly due to the structural changes made by incorporation of APP into the GNP layers. It can be concluded that the efficiency of GNP-g-APP was more that GNP in EVA and probably GNP-g-APP could act in both gas and condensed phases, which encouraged us for further analyses.

3.2.5. *Mass loss cone calorimeter (MLC)*

Fig. 13 shows HRR curves as a function of fire exposure time for EVA and its composites. Table 5 summarizes the obtained results. The incorporation of GNP induced a significant reduction in pHRR of about −46% without affecting the TTI that remained very close to that of pristine EVA (52 s). THR was also reduced when GNP was used (−14.5%). The enhancement of EVA flame retardant properties was more significant by the use of GNP-g-APP. In fact, pHRR and THR reductions were more pronounced by values of −63% and −31.6%, respectively. However, TTI was significantly decreased by the incorporation of 30 wt.% GNP-g-APP into EVA compared to what happened in the case of EVA/GNP30. This result was related to the decline in the thermal stability of this composite highlighted by the superposition of the DTG curves of EVA, EVA/GNP30 and EVA/GNP-g-APP (Fig. 12). The premature decomposition was not corresponding to the gases released by phase action compounds, but correlated to combustible volatiles. Condensed

Table 5 – Result of MLC tests performed on EVA samples.

Name	TTI (s)	pHRR (kW/m^2)	pHRR reduction (%)	THR (kJ/g)	THR reduction (%)
EVA	52	940	–	117	–
EVA/GNP30	56	510	−46	100	−14.5
EVA/GNP-g-APP30	30	340	−63	80	−31.6

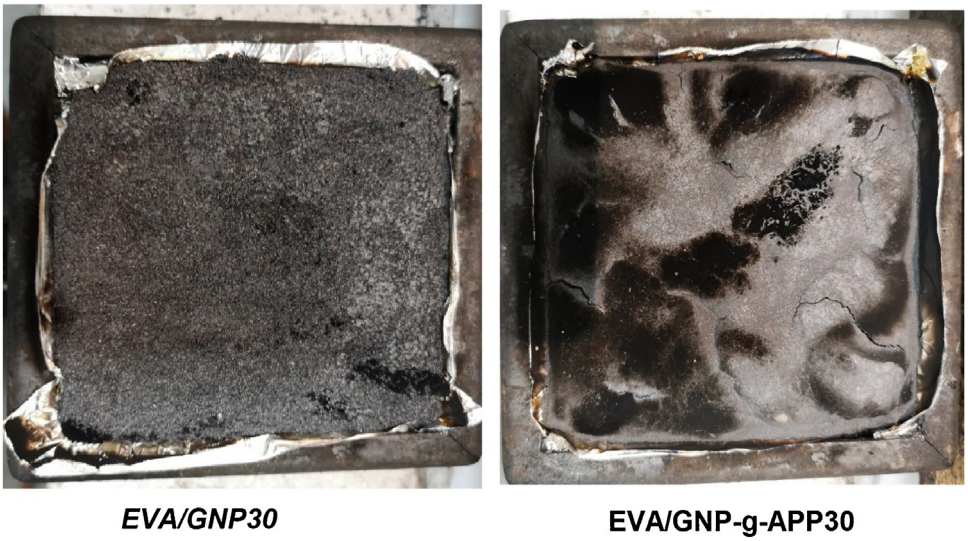

Fig. 14 – Digital images of the combustion residue obtained after MLC test on EVA/GFP30 and EVA/GFP-g-APP 30.

Table 6 – Mechanical properties of EVA samples.

Samples	Stress at break (kg/cm^2)	Elongation at break (%)
EVA	101	499
EVA/GNP30	43	71
EVA/GNP-g-APP30	64	364

phase action of GNP-g-APP in the EVA offered the main mode of action responsible for enhancing the flame retardant properties of composite. It is particularly visible on the images of residues formed during MLC tests. Fig. 14 suggests that the combustion residue of the composite containing GNP-g-APP had higher cohesion with respect to that formed during the combustion of EVA/GNP30 (mainly composed of black powder that does not present any cohesion). The presence of phosphorus improved the barrier effect of the char and; thus, enabled the sample to approach further pHRR reduction.

3.2.6. *Mechanical properties*

The mechanical properties of the neat EVA and its composites were studied by applying tensile tests (Fig. 15). The average values of mechanical characteristics of samples are reported in Table 6. The neat EVA showed an average stress at break of ca. 100 kg/cm^2 and the elongation of ca. 500%. About EVA/GNP30, the stress and elongation at break values were 43 kg/cm^2 and 71% respectively (Table 6), which showed about 57% fall in stress at break and more than 76% reduction in elongation at break. This was a signature of incompatibility of GNP with EVA. When 30 wt.% of GNP-g-APP was used in EVA, the elongation and stress at break values reached 364% and 64 kg/cm^2, respectively. This revealed that the flexibility of this composite was preserved to some extent compared to the neat EVA. In the other word, particles of GNP-g-APP had a higher interfacial adhesion to EVA matrix.

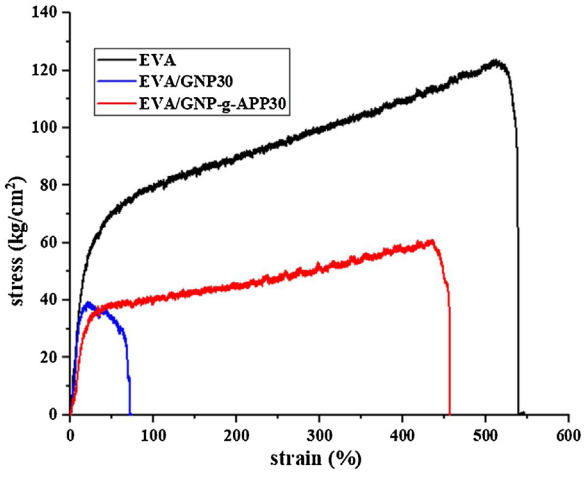

Fig. 15 – Tensile Stress–Strain curves for EVA samples.

4. Conclusions

GNP-g-APP was synthesized by functionalization of exfoliated graphite nanoplatelet (GNP), fully characterized, and applied as flame retardant additive in EVA matrix. The results of FTIR, SEM, and EDS analyses proved that 6.5 wt.% APP phosphorus precursor was grafted onto the surface of GNP. TGA results confirmed that GNP-g-APP promoted char effect at high tem-

perature (20.2% at 800), unlike GNP with limited potential for making EVA flame retardant. After applying 30 wt.% of GNP-g-APP, UL94 analysis implied V-0 rating, in contrast to the neat EVA and EVA composite containing the same amount of GNP with non-rating labels. Moreover, the TGA result showed that residue at 800 °C increased from ca. 26.5 wt.% for GNP30 to 31.1 wt.% for GNP-*g*-APP. Flame retardation effect of GNP-g-APP on EVA was further confirmed by PCFC test, showing obvious reduction in THR and pHRR of the neat EVA polymer. Mass Loss Cone Calorimeter results revealed a reduction of 45% in the value of pHRR for EVA/GNP30, and −63% fall of pHRR of EVA/GNP-g-APP30, with respect to the neat EVA. According to the literature, EVA composites containing 30 wt.% APP/poly(piperazinyl malonamide) showed −50% fall in the pHRR, and for the EVA containing 30 wt.% graphene oxide the difference was −63% [50], which is indicative of superiority of the flame retardant developed in the present work. The flexibility of composite was conserved to some extent compared to the neat EVA by using GNP-g-APP due to improved compatibility with EVA. The tensile strength of EVA/GNP-g-APP30 was 36% lower than that of EVA, while the value for EVA/GNP30 was 57% lower than neat EVA. However, the tensile strength of EVA/GNP-g-APP30 was about 50% higher than that of EVA/GNP30; moreover, the elongation at break in the same order was more that 500% higher for the EVA/GNP-g-APP30.

Funding

This research did not receive any specific grant from funding agencies in the public, commercial, or not-for-profit sectors.

Declaration of interests

The authors declare that they have no known competing financial interests or personal relationships that could have appeared to influence the work reported in this paper.

REFERENCES

[1] Schneider C, Langer R, Loveday D, Hair D. Applications of ethylene vinyl acetate copolymers (EVA) in drug delivery systems. Control Release 2017;262:284–95.
[2] Liu S, Kong Y, Wan T, Zhao G. Effects of thermal-cooling cycling curing on the mechanical properties of EVA-modified concrete. Constr Build Mater 2018;165:443–50.
[3] Ramesh S, Punithamoorthy K. Synthesis, characterization and gas permeability properties of a novel nanocomposite based on poly (ethylene-co-vinyl acetate)/polyurethane acrylate/clay. J Mater Res Technol 2019;8:4173–81.
[4] Park Y, Joo H, Kim H, Lee Y. Adhesion and rheological properties of EVA-based hot-melt adhesives. J Adhes Adhes 2006;26:571–6.
[5] Vahabi H, Raveshtian A, Fasihi M, Sonnier R, Saeb MR, Dumazert L, et al. Competitiveness and synergy between three flame retardants in poly (ethylene-co-vinyl acetate). Polym Degrad Stab 2017;143:164–75.
[6] Omri N, Oualha MA, Vahabi H, Amdouni N, Abderrabba M, Laoutid F. Promising effect of combining [60]Fullerene nanoparticles and calcium hydroxide on thermal stability and flammability of Poly (ethylene-co-vinyl acetate). Thermochim Acta 2018;668:73–9.
[7] Ramesan MT. Poly (Ethylene-Co-Vinyl acetate)/magnetite nanocomposites: interaction of some liquid fuels, thermal and oil resistance studies. Polym Compos 2015;23:85–92.
[8] Ramesan M. Fabrication, characterization, and properties of poly (ethylene- co- vinyl acetate)/magnetite nanocomposites. J Appl Polym Sci 2014;131.
[9] Ramesan MT. Dynamic mechanical properties, magnetic and electrical behavior of iron oxide/ethylene vinyl acetate nanocomposites. Polym Compos 2014;35:1989–96.
[10] Covaci A, Harrad S, Abdallah MAE, Ali N, Law RJ, Herzke D, et al. Novel brominated flame retardants: a review of their analysis, environmental fate and behaviour. Environ Int 2011;37:532–56.
[11] Shaw S. Halogenated flame retardants: do the fire safety benefits justify the risks? Rev Environ Health 2010;25:261–306.
[12] Witkowski A, Hollingbery L, Hull TR. Fire retardancy of mineral fillers in EVA copolymers. In: Fire and polymers VI: new advances in flame retardant chemistry and science; 2012. p. 97–111.
[13] Oualha MA, Amdouni N, Laoutid F. Synergistic flame-retardant effect between calcium hydroxide and zinc borate in ethylene-vinyl acetate copolymer (EVA). Polym Degrad Stab 2017;144:315–24.
[14] Rakotomalala M, Wagner S, Döring M. Recent developments in halogen free flame retardants for epoxy resins for electrical and electronic applications. J Mater 2010;3:4300–27.
[15] Baldissera AF, da Silva Silveira MR, Beraldo CH, Tocchetto NS, Ferreira CA. Polymeric organic coatings based on PANI-ES and PANI-ES/APP for fire protection. J Mater Res Technol 2019;8:2832–45.
[16] Vahabi H, Paran SMR, Shabanian M, Dumazert L, Sonnier R, Movahedifar E, et al. Triple-faced polypropylene: fire retardant, thermally stable, and antioxidative. J Vinyl Addit Techn 2019;25:366–76.
[17] Mehrali M, Latibari ST, Mehrali M, Mahlia TMI, Metselaar HSC, Naghavi MS, et al. Preparation and characterization of palmitic acid/graphene nanoplatelets composite with remarkable thermal conductivity as a novel shape-stabilized phase change material. Appl Therm Eng 2013;61:633–40.
[18] Rao W-H, Liao W, Wang H, Zhao H-B, Wang Y-Z. Flame-retardant and smoke-suppressant flexible polyurethane foams based on reactive phosphorus-containing polyol and expandable graphite. J Hazard Mater 2018;360:651–60.
[19] Wu X, Wang L, Wu C, Yu J, Xie L, Wang G, et al. Influence of char residues on flammability of EVA/EG, EVA/NG and EVA/GO composites. Polym Degrad Stab 2012;97:54–63.
[20] Shen MY, Chen WJ, Tsai KC, Kuan CF, Kuan HC, Chou HW, et al. Preparation of expandable graphite and its flame retardant properties in HDPE composites, Ṗreparation of expandable graphite and its flame retardant properties in HDPE composites. Polym Compos 2017;38:2378–86.
[21] Tang M, Chen M, Xu Y, Chen X, Sun Z, Zhang Z. Combustion characteristics and synergistic effects of red phosphorus masterbatch with expandable graphite in the flame retardant HDPE/EVA composites. Polym Eng Sci 2015;55:2884–92.
[22] Wang Z, Han E, Ke W. Influence of expandable graphite on fire resistance and water resistance of flame-retardant coatings. Corros Sci 2007;49:2237–53.
[23] Zhang XG, Ge LL, Zhang WQ, Tang JH, Ye L, Li ZM. Expandable graphite-methyl methacrylate-acrylic acid copolymer composite particles as a flame retardant of rigid polyurethane foam. J Appl Polym Sci 2011;122:932–41.

[24] Zheng J, Li B, Guo C, Wu Q, Wang Y. Flame-retardant properties of acrylonitrile–butadiene–styrene/wood flour composites filled with expandable graphite and ammonium polyphosphate. J Appl Polym Sci 2014;131.
[25] Wang J, Ma C, Mu X, Cai W, Liu L, Zhou X, et al. Construction of multifunctional MoSe2 hybrid towards the simultaneous improvements in fire safety and mechanical property of polymer. J Hazard Mater 2018;352:36–46.
[26] Zhou S, Zhou Y, Ling Z, Zhang Z, Fang X. Modification of expanded graphite and its adsorption for hydrated salt to prepare composite PCMs. Appl Therm Eng 2018;133:446–51.
[27] Vallejo J, Álvarez-Regueiro E, Cabaleiro D, Fernández-Seara J, Fernández J, Lugo L. Functionalized graphene nanoplatelet nanofluids based on a commercial industrial antifreeze for the thermal performance enhancement of wind turbines. Appl Therm Eng 2019;152:113–25.
[28] Yang L, Liu H, Deng Q, Zhou YZ, Zhang YZ. Modification of expandable graphite and adsorption for methyl orange. Appl Mech Mater 2014;618:81–5.
[29] Zhao S, Li P, Adkins J, Zhu L, Du F, Zhou Q, et al. Carboxyl grafted sulfur-expanded graphite composites as cathodes for lithium-sulfur batteries. J Electroanal Chem 2018;823:422–8.
[30] Wang Y, Wang F, Dong Q, Xie M, Liu P, Ding Y, et al. Core-shell expandable graphite@ aluminum hydroxide as a flame-retardant for rigid polyurethane foams. Polym Degrad Stab 2017;146:267–76.
[31] Zhu H, Zhu Q, Li J, Tao K, Xue L, Yan Q. Synergistic effect between expandable graphite and ammonium polyphosphate on flame retarded polylactide. Polym Degrad Stab 2011;96:183–9.
[32] Zhang M, Ding X, Zhan Y, Wang Y, Wang X. Improving the flame retardancy of poly (lactic acid) using an efficient ternary hybrid flame retardant by dual modification of graphene oxide with phenylphosphinic acid and nano MOFs. J Hazard Mater 2020;384:121260.
[33] Wang H, Cao J, Cao C, Guo Y, Luo F, Qian Q, et al. Influence of phosphorus-grafted expandable graphite on the flame-retardant property of UHMWPE composite. Polym Adv Technol 2019;30:493–503.
[34] Movahedifar E, Vahabi H, Saeb MR, Thomas S. Flame retardant epoxy composites on the road of innovation: an analysis with flame retardancy index for future development. Molecules 2019;24:3964.
[35] Tikhani F, Moghari S, Jouyandeh M, Laoutid F, Vahabi H, Saeb MR, et al. Curing kinetics and thermal stability of epoxy composites containing newly obtained nano-scale aluminum hypophosphite (AlPO2). J Polym 2020;12:644.
[36] Vahabi H, Laoutid F, Movahedifar E, Khalili R, Rahmati N, Vagner C, et al. Description of complementary actions of mineral and organic additives in thermoplastic polymer composites by Flame Retardancy Index. Polym Adv Techno 2019;30:2056–66.
[37] Fang F, Song P, Ran S, Guo Z, Wang H, Fang Z. A facile way to prepare phosphorus-nitrogen-functionalized graphene oxide for enhancing the flame retardancy of epoxy resin. Compos Commun 2018;10:97–102.
[38] Fang F, Ran S, Fang Z, Song P, Wang H. Improved flame resistance and thermo-mechanical properties of epoxy resin nanocomposites from functionalized graphene oxide via self-assembly in water. Compos B Eng 2019;165:406–16.
[39] Huang G, Han D, Jin Y, Song P, Yan Q, Gao C. Fabrication of nitrogen-doped graphene decorated with organophosphor and lanthanum toward high-performance ABS nanocomposites. ACS Appl Nano Mater 2018;1:3204–13.
[40] Jin Y, Huang G, Han D, Song P, Tang W, Bao J, et al. Functionalizing graphene decorated with phosphorus-nitrogen containing dendrimer for high-performance polymer nanocomposites. Compos A Appl Sci Manuf 2016;86:9–18.
[41] Ran S, Fang F, Guo Z, Song P, Cai Y, Fang Z, et al. Synthesis of decorated graphene with P, N-containing compounds and its flame retardancy and smoke suppression effects on polylactic acid. Compos B Eng 2019;170:41–50.
[42] Shao Z, Deng C, Tan Y, Chen M, Chen L, Wang Y. An efficient mono-component polymeric intumescent flame retardant for polypropylene: preparation and application. Appl Mater Inerface 2014;6:7363–70.
[43] Vahabi H, Kandola BK, Saeb MR. Flame retardancy index for thermoplastic composites. Polymers 2019;11:407.
[44] Rochman RA, Wahyuningsih S, Ramelan AH, Hanif QA. Preparation of nitrogen and sulphur Co-doped reduced graphene oxide (rGO-NS) using N and S heteroatom of thiourea. IOP Conf Ser Mater Sci Eng 2019;509:012119.
[45] Xu T, Li Y, Chen J, Wu H, Zhou X, Zhang Z. Improving thermal management of electronic apparatus with paraffin (PA)/expanded graphite (EG)/graphene (GN) composite material. Appl Therm Eng 2018;140:13–22.
[46] Emami A, Ghafuri H, Kenari MK, Maleki A. Investigating the catalytic performance of graphene oxide–polyaniline–lignosulfonate nanocomposite in the synthesis of polysubstituted pyridines via a four – component reaction. Chem Select 2018;3:6349–57.
[47] Riva A, Camino G, Fomperie L, Amigouet P. Fire retardant mechanism in intumescent ethylene vinyl acetate compositions. Polym Degrad Stab 2003;82:341–6.
[48] McGarry K, Zilberman J, Hull TR, Woolley WD. Decomposition and combustion of EVA and LDPE alone and when fire retarded with ATH. Polym Int 2000;49:1193–8.
[49] Shi Y, Kashiwagi T, Walters RN, Gilman JW, Lyon RE, Sogah DY. Ethylene vinyl acetate/layered silicate nanocomposites prepared by a surfactant-free method: enhanced flame retardant and mechanical properties. Polymer 2009;50:3478–87.
[50] Vahabi H, Gholami F, Karaseva V, Laoutid F, Mangin R, Sonnier R, et al. Novel nanocomposites based on poly (ethylene-co-vinyl acetate) for coating applications: the complementary actions of hydroxyapatite, MWCNTs and ammonium polyphosphate on flame retardancy. Prog Org Coat 2017;113:207–17.